INTERNATIONAL JOURNAL OF ROBOTICS
(THEORY AND APPLICATIONS)
E-mail: IJR@kntu.ac.ir

Experiments on a Novel Hybrid Elastic Joint Robot with a Robust and Fast Control Strategy for Minimally Invasive Surgery

M. Souzanchi-K[a], M-R. Akbarzadeh-T[b,*]

[a] Center of Excellence on Soft Computing and Intelligent Information Processing, Department of Electrical Engineering, Ferdowsi University of Mashhad, Mashhad, Iran
[b] Center of Excellence on Soft Computing and Intelligent Information Processing, Department of Electrical Engineering, Ferdowsi University of Mashhad, Mashhad, Iran

ARTICLE INFO

Article history:
Submit: 2021-01-17
Revise: 2021-11-03
Accept: 2022-02-26

Keywords:
Minimally invasive surgery
Elastic joint hybrid robot
Voltage control
Adaptive fuzzy estimator

ABSTRACT

Design and control of surgical robots for minimally invasive surgery have considerable challenges in handling unknown robot dynamics, environmental uncertainties, desirable workspaces, and fast motion reactions. Realistic operational requirements regarding kinematics and dynamics of the robot and its actuators also lead to joint elasticity; therefore, further concerns regarding sustained chattering, vibration, and instability are raised. Accordingly, the robot proposed here is designed based on a hybrid structure, consisting of two parallel and serial manipulators, aiming for the desired rigidity and acceptable manipulability requirements of robotic surgeries. Furthermore, a decentralized sliding mode controller with an indirect adaptive fuzzy estimator based on a voltage control strategy is employed to tackle the challenges of controlling such as chattering phenomenon, control loop's speed, and stability against uncertainties. In contrast to the traditional sliding mode controllers, the control law is free from robot dynamics, the control signals' chattering is reduced, and bounded input-bounded output stability is shown without knowing the uncertainty bounds on robot dynamics. Simulation and experimental studies indicate that this approach is realistic.

* Corresponding address: Department of Electrical Engineering, Ferdowsi University of Mashhad, Mashhad, Iran
Tel.: +98 5138805010
E-mail address: akbarzadeh@ieee.org

1. Introduction

Minimally Invasive Surgery (MIS) is a medical procedure that makes small incisions (less than 10mm in diameter) and performs surgery using the laparoscopic instruments inserted through small-diameter trocars placed at the incisions. Reducing patient trauma, reducing bleeding during surgery, reducing damage to the body's tissues, faster recovery, and fewer healthcare costs are advantages of MIS than traditional open surgery. Robot manipulators are increasingly being used in surgical operations to improve the accuracy and comfort of the surgical processes because they can remove tremors of the surgeon's hand, reduce fatigue of the surgeon's eyes, and increase the doctor's reachability. This means increasing maneuverability of both hands, 360º wrist rotations, and 3D visualization. Therefore, robotic-assisted minimally invasive surgery has brought innovations into MIS and has enhanced surgeons' capabilities by coupling their knowledge with robotic manipulability. Meanwhile, robots have some disadvantages in this process, including a higher initial cost, higher maintenance, and longer setup time. Still, in the tradeoff between advantages and disadvantages, the advantages outweigh the disadvantages.

The robots that used in MIS can be classified into two categories: the first integrates the laparoscope holders such as the AESOP [1] and PARAMIIS laparoscope manipulators [2], and the second act as the assistant to the surgeons such as HERMES, Zeus, Hansen's Sensei, and da Vinci [3]. In addition to these divisions, small and individual surgical robots have been considered, such as miniature parallel robots for spine and trauma surgery, directly mounted on the patient's bone [4]. Recent research [5-9] shows that surgical robots are currently an exciting research topic, and new research directions lead to the development of new robotic surgery devices in the future.

This paper designs an elastic joint hybrid robot, a combination of parallel and serial robots, which resolve some challenges in the currently developed systems. This combination benefits from the parallel robots' accuracy and the manipulability of the serial robot's workspace. Torque mode control is the typical strategy that uses for surgical robots. Most of the control approaches assume precisely the knowledge of the robot dynamics. However, this knowledge may be unavailable. Due to the nonlinearity and coupling in the surgical robots' dynamics, designing a controller based on torque mode control strategy is complicated and often carries high computational complexity.

Furthermore, these schemes often ignore their electric actuators' dynamics, whereas these actuators have an essential role in performing high-precision tasks. The transmission system's deformation further produces elasticity in the joints, which is the main source of vibration or even instability in robots [10]. It also presents additional complexity and nonlinearity through its input-output coupling. Hence, high precision applications of an elastic joint robot seem to be difficult since the link position does not directly follow the actuator position. In other words, the degrees of freedom become twice the number of control actions. Additionally, the controllers based on torque mode strategy need one more control loop to produce the desired torque by controlling the actuators' current.

To overcome the stated shortcomings, this paper uses a voltage mode control strategy that is free from robot dynamics [11]. This strategy is an evolving field of research, accepted worldwide due to its advantages. Adaptive Taylor series control [12], robust control [13], impedance control [14], adaptive control [15], and approximation control [16] show the superiority of this strategy. These theories have been implemented on the serial robot, but the voltage mode control strategy is used on the hybrid surgical robot for the first time in this paper.

Sliding mode control is often used to guarantee systems' stability with unknown dynamics, parametric uncertainties, and noise in the available output, such as a robotic system [17-19]. However, these controllers lead to undesirable chattering while reaching good theoretical results. Furthermore, they require the limits of uncertainty to be known. To gain mastery over this difficulty, this paper presents a novel sliding mode control based on voltage control strategy, in which an indirect adaptive fuzzy estimator is used for the elastic joint hybrid surgical robot. This is in contrast to recent work by authors in which brain emotional learning is used to estimate the robot dynamics [20], and the computational closed-loop control cycle in this work is shorter than [20]. This method carries more straightforward dynamics while also being more effective than the torque mode control strategy. Finally, the bound of uncertainty is not necessary for this approach.

Another novelty of this controller is that it uses one control loop to control the joint angles directly instead of using two control loops used in most previous controllers. This paper aims to design a chatter-free and stable control law, using the least knowledge about the robot dynamics while lowering the computational burden.

This paper is organized into the following sections. Section 2 discusses the elastic joint hybrid surgical robot's modeling. The proposed

control architecture is introduced in Section 3. Section 4 provides a theoretical stability analysis of the closed-loop system. Simulation results, comparisons with a competing strategy, and experimental results are provided in Section 5. Finally, conclusions are drawn, and avenues for future work are discussed in Section 6.

Table 1. List of acronyms

Symbol	Description
q	The vector of joint angles
θ_m	The vector of rotor angles
$D(q)$	Inertia matrix of the manipulator
$C(q,\dot{q})\dot{q}$	Vector of centrifugal and Coriolis forces
$G(q)$	The vector of gravitational forces
τ_m	Torque vector of motors
J	Motor inertia
B	Motor damping
r	Reduction gear
K	Lumped flexibility of the joint and reduction gear
V	The vector of motor voltages
I_a	The vector of motor currents
R	Armature resistance
L	Armature inductance
K_b	Back-emf constant
K_m	Torque constants diagonal matrix
X	State vector
n	The number of mobile element
m	The number of one DOF joint
T	The time of operation
μ	A parameter of the desired trajectory
ϑ	A parameter of the desired trajectory
s	Sliding surface
e	The tracking error
λ	A constant and positive coefficient
β	A constant and positive coefficient
ε	Approximation error
μ_{A_l},μ_{B_l}	Input membership function
μ_{C_l}	Output membership function
$\hat{y}_l$	The center of C_l

2. Robot kinematic design and modeling

Robots lose their generality for different surgeries with smaller workspaces, while larger workspaces lower the operation accuracy; therefore, workspace is an essential issue for the surgical robot, and some researchers focus on this subject [21-24].

In this paper, a new hybrid surgical robot shown in Fig.1 is designed to be used in MIS applications such as abdominal and urology surgeries. This robot consists of two main subsystems: a parallel manipulator used here as a base for its inherent properties such as accuracy and rigidity, and a serial manipulator used for its improved robot's workspace and manipulability of the active instruments, such as cutting, suturing, and grasping. It is necessary to mention that the serial manipulator is extensively discussed by [10], while the rest of this section addresses parallel robot modeling.

According to the surgical operation, higher accuracy, higher load-to-weight ratio, and more miniature size robots are necessary; therefore, a Revolute Spherical Universal (RSU) structure is designed for the parallel robot. The moving and base platforms are connected with six limbs and six RSU structures. Finally, the serial robot is located on the moving platform.

To determine the total number of Degree of Freedom (DOF) for this hybrid surgical robot, we should find the DOF of each part separately. The serial robot has three revolute joints; therefore, the number of DOF is 3; the details of the DOF analysis can be found in [25]. To find the DOF of the parallel robot, we used the Grubler-Chebyshev-Kutzbach relation that is expressed as,

$$DOF = 6n - 5m, \tag{1}$$

According to Table 1, n is the number of mobile elements, and m is the number of one DOF joints. Due to Fig.2, which illustrates the RSU structure, in each chain, five rigid elements exist in addition to the base platform, and the moving platform is another one; therefore, the number of the mobile element is $n = 6 * 5 + 1 = 31$, and the number of one DOF joint is $m = 6 * 6 = 36$. Therefore by using (1), the DOF of the parallel robot be obtained as follows,

$$DOF = 6 * 31 - 5 * 36 = 6. \tag{2}$$

Eventually, the total number of DOF for the hybrid surgical robot is,

$$DOF = 3 + 6 = 9. \tag{3}$$

According to the nine DOF, nine DC motors are used to drive this robot, i.e., each revolute joint has a separate actuator. We consider the actuator dynamics and robot dynamics for more accurate and realistic modeling and use a power transmission mechanism between the robot and the actuator. Due to the gear's presence in the power transmission systems and joints moving in

different directions, elasticity is created; therefore, a linear torsional spring is used to model the joint elasticity. This phenomenon is the source of vibration and instability in robot movement. Furthermore, the robot model is a highly nonlinear, computationally extensive, strongly coupled, and multi-input/multi-output system with $2n$ coordinates. These complexities have been a considerable challenge in robot modeling and control.

Integrated state-space modeling is introduced in this paper using the dynamics and kinematics of robots, including actuator modeling. According to [10], the dynamic equation of the robot can be shown as,

$$D(q)\ddot{q} + C(q,\dot{q})\dot{q} + G(q) = K(r\theta_m - q), \quad (4)$$

$$J\ddot{\theta}_m + B\dot{\theta}_m + rK(r\theta_m - q) = \tau_m, \quad (5)$$

where $\theta_m = [\theta_{mp}\ \theta_{ms}]$ and $q = [q_p\ q_s]$ are the vector of the rotor and joint angles, individually, also the sub-indexes $\{p, s\}$ are used for parallel and serial manipulators, respectively. Therefore, this framework has $2n$ coordinates as $[q, \theta_m]$.

Also, $D(q) \in R^{n\times n}$ is the inertia matrix of the manipulator, $C(q,\dot{q})\dot{q} \in R^n$ is the vector of centrifugal and Coriolis forces, $G(q) \in R^n$ is the vector of gravitational forces and $\tau_m \in R^n$ is the vector of the motor's torque. J, B, and $r \in R^{n\times n}$ are the diagonal matrices represent the coefficients of the motor inertia, motor damping, and reduction gear, respectively. The diagonal matrix K represents the lumped elasticity of the joints and reduction gears together.

The generalized coordinates are separated into two sets as $q = [q_p\ q_s]$. So we have, $D(q) = \begin{bmatrix} D_p & D_{ps} \\ D_{sp} & D_s \end{bmatrix}, C(q,\dot{q}) = \begin{bmatrix} C_p & C_{ps} \\ C_{sp} & C_s \end{bmatrix}, G(q) = \begin{bmatrix} G_p \\ G_s \end{bmatrix}$. To obtain the motor voltage as an input, consider the electrical equation of the DC motors in the below matrix form,

$$R_a I_a + L_a \dot{I}_a + K_b \dot{\theta}_m = V, \quad (6)$$

due to Table 1, $V \in R^n$ is the vector of motor voltages, $I_a \in R^n$ is the vector of motor currents and $\dot{\theta}_m$ is the vector of rotor velocities. $R_a, L_a, K_b \in R^{n\times n}$ represent the diagonal matrices for the coefficients of armature resistance, armature inductance, and back-emf constant, respectively. Motor torques τ_m as input for (5) is produced by the motor currents vector, as follows,

$$\tau_m = K_m I_a, \quad (7)$$

where K_m is the diagonal matrix of the torque constants. Equations (4)-(7) form the robotic system so that the voltage vector V is the input vector, and the joint angle vector q is the output vector. Utilizing (4)-(7), the state-space model of the electrically driven elastic joint hybrid surgical robot can be derived as,

Figure 1. Hybrid surgical robot

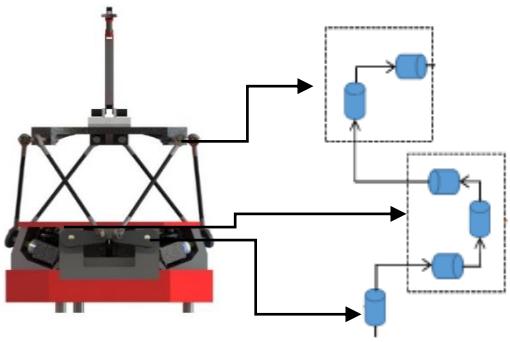

Figure 2. RSU kinematic chain

$$\dot{X} = f(X) + bV, \quad (8)$$

$$f(X) = \begin{bmatrix} X_2 \\ D^{-1}(X_1)(-G(X_1) - KX_1 - C(X_1, X_2)X_2 + KrX_3) \\ X_4 \\ J^{-1}(rKX_1 - r^2KX_3 - BX_4 + K_mX_5) \\ -L^{-1}(K_bX_4 + RX_5) \end{bmatrix},$$

$$b = \begin{bmatrix} 0 \\ 0 \\ 0 \\ 0 \\ L^{-1} \end{bmatrix} \quad X = \begin{bmatrix} q \\ \dot{q} \\ \theta_m \\ \dot{\theta}_m \\ I_a \end{bmatrix}. \quad (9)$$

Equations (8) and (9) show a coupled nonlinear multivariable system. The complexity of the model has been a severe challenge in this paper. Hence, modeling and controlling this robot is an appropriate challenge to show the proposed control method's art in the surgical robot field.

3. Proposed controller

A stable decentralized sliding mode controller with an indirect adaptive fuzzy estimator is proposed based on the voltage control strategy. To design the sliding mode controller, the electrical equation of each motor that given by (6) should be

changed to the standard model; therefore, one of the novelties of this paper is that prepared this model by using the joint velocity, (6) can be represented as,

$$\dot{q} - \dot{q} + RI_a + L\dot{I}_a + K_b\dot{\theta}_m = V. \quad (10)$$

The system (10) is re-expressed as,

$$\dot{q} + H = V, \quad (11)$$

Function H is expressed as,

$$H = RI_a + L\dot{I}_a + K_b\dot{\theta}_m - \dot{q}. \quad (12)$$

The sliding surface that use to design the controller is defined as,

$$s = e + \lambda \int e \ dt \ , \quad (13)$$

where e is the tracking error represented by,

$$e = q_d - q, \quad (14)$$

in which q_d and q are the desired and actual joint angles, successively and λ in (13) is a constant and positive coefficient.

A positive definite function Λ is suggested to obtain the control law,

$$\Lambda = \frac{1}{2}s^2. \quad (15)$$

The derivative of the above positive definite function with respect to time is calculated as,

$$\dot{\Lambda} = s\dot{s}. \quad (16)$$

If $\dot{\Lambda} < 0$ then $s \to 0$. Hence, let

$$s\dot{s} = -\beta|s|, \quad (17)$$

$$\dot{s}sgn(s) = -\beta, \quad (18)$$

where β is a constant and positive coefficient and $sgn(s) = s/|s|$. $\dot{s}$ is calculated by using (13) and substituting into (18) yields,

$$(\dot{e} + \lambda e)sgn(s) = -\beta. \quad (19)$$

By replacing (11) in to (19),

$$(\dot{q}_d + H - V + \lambda e)sgn(s) = -\beta, \quad (20)$$

where H is formulated as,

$$H = \overline{H} + \Delta H, \quad (21)$$

$$\overline{H} = -\dot{q}, \quad (22)$$

$$\Delta H = RI_a + L\dot{I}_a + K_b\dot{\theta}_m. \quad (23)$$

Based on two reasons, the effect of $L\dot{I}_a$ is ignorable. The first one is that the electrical time constant of the DC motor is significantly smaller than its mechanical time constant, and the second is that $\dot{I}_a$ might be noisy, and measuring is not recommended [26]. Therefore,

$$\overline{\Delta H}(I_a, \dot{\theta}_m) \approx RI_a + K_b\dot{\theta}_m. \quad (24)$$

By substituting (22) and (24) to (21) and then (21) to (20),

$$\left(\dot{q}_d + \overline{H} - V + \lambda e + \overline{\Delta H}(I_a, \dot{\theta}_m)\right)sgn(s) = -\beta. \quad (25)$$

Control law V is calculated by multiplying both sides of (25) in $sgn(s)$,

$$V = \dot{e} + \lambda e + \overline{\Delta H}(I_a, \dot{\theta}_m) + \beta sgn(s). \quad (26)$$

Computing the uncertainty limitation is one of the sliding mode controller challenges. To overcome this shortcoming in this paper, the indirect adaptive fuzzy estimator is employed to estimate $\overline{\Delta H}(I_a, \dot{\theta}_m)$.

The vectors of motor current and rotor velocity are considered as input of adaptive fuzzy estimator,

$$x_1 = I_a, \quad (27)$$

$$x_2 = \dot{\theta}_m. \quad (28)$$

By assigning three membership functions to each fuzzy input, the whole space is covered by nine fuzzy rules. To obtained the fuzzy linguistic rules, the Mamdani type is used,

$$Rule\ l\text{: If } \ x_1 \text{is } A_l \text{ and } \ x_2 \text{ is } B_l \text{ Then } \overline{\Delta H} \text{ is } C_l, \quad (29)$$

where $Rule\ l$ with $l = 1, \dots, 9$, denotes the lth fuzzy rule. In the lth rule, A_l, B_l, and C_l are fuzzy membership functions for variables x_1, x_2 and V, respectively. However, since the precise information on the ranges of x_1 and x_2 are not provided, S shape and Z shape membership functions are employed for P and N, respectively. These three functions are expressed as,

$$\mu_p(x_1) = \begin{cases} 0 & x_1 \le 0 \\ 2x_1^2 & 0 \le x_1 \le 0.5 \\ 1 - 2(x_1 - 1)^2 & 0.5 \le x_1 \le 1 \\ 1 & x_1 \ge 1 \end{cases},$$

$$\mu_N(x_1) = \begin{cases} 1 & x_1 \le -1 \\ 1 - 2(x_1 + 1)^2 & -1 \le x_1 \le -0.5 \\ 2x_1^2 & -0.5 \le x_1 \le 0 \\ 0 & x_1 \ge 0 \end{cases},$$

$$\mu_Z(x_1) = exp\left(\frac{-x_1^2}{2\sigma^2}\right) \qquad \sigma = 0.3. \quad (30)$$

The membership functions for x_2 are similar to x_1. The Gaussian membership functions are determined for the output expressed by,

$$\mu_{C_l}(\overline{\Delta H}) = exp\left(-\left(\frac{(\overline{\Delta H} - \hat{y}_l)^2}{2\sigma^2}\right)\right), \quad (31)$$

where $\hat{y}_l$ is the center of C_l. If we use the Mamdani inference engine, singleton fuzzifier, and center average defuzzifier, along with (29)-(31), $\overline{\Delta H}$ is calculated by [27],

$$\overline{\Delta H} = \sum_{l=1}^{9} \hat{y}_l \psi_l(x_1, x_2) = \hat{y}^{\mathrm{T}} \psi(x_1, x_2), \quad (32)$$

where $\psi = [\psi_1 \dots \psi_9]^T$ in which ψ_l is called a fuzzy basis that is a positive value expressed as:

$$\psi_l(x_1, x_2) = \frac{\mu_{A_l}(x_1)\mu_{B_l}(x_2)}{\sum_{l=1}^{9} \mu_{A_l}(x_1)\mu_{B_l}(x_2)}, \quad (33)$$

where $\mu_{A_l}, \mu_{B_l} \in [0,1]$; therefore, $|\psi_l(x_1, x_2)| \le 1$, hence fuzzy function ψ is bounded. Parameters $\hat{y}$ in (32) are determined by the adaptive rule afterward.

Fuzzy systems can be considered as general estimators, therefore,

$$\Delta H = \mathrm{y}^{\mathrm{T}}\psi(x_1, x_2) + \epsilon, \quad (34)$$

where y is the desired value of $\hat{y}$ and ϵ is the estimation error that is bounded according to the general approximate theorem [10].

The following closed-loop control system is obtained by substituting control low (26) to the system (11).

$$\dot{q} + H = \dot{e} + \lambda e + \overline{\Delta H}(I_a, \dot{\theta}_m) + \beta sgn(s), \quad (35)$$

by substituting (11), (22), (32) and (34) into (35),

$$\dot{e} = -\lambda e - \beta sgn(s) + (\mathrm{y}^{\mathrm{T}} - \hat{\mathrm{y}}^{\mathrm{T}})\psi(x_1, x_2) + \epsilon. \quad (36)$$

To obtain the adaptive law, a positive definite function w is suggested as,

$$w = \frac{1}{2}e^2 + \frac{1}{2\beta}(y^T - \hat{y}^T)(y - \hat{y}). \quad (37)$$

The derivative of the positive definite function w with respect to time is calculated as,

$$\dot{w} = e\dot{e} - \frac{1}{\beta}(y^T - \hat{y}^T)\dot{\hat{y}}. \quad (38)$$

by substituting (36) into (38),

$$\dot{w} = -\lambda e^2 + e\big((y^T - \hat{y}^T)\psi + \epsilon - \beta sgn(s)\big) - \frac{1}{\beta}(y^T - \hat{y}^T)\dot{\hat{y}} \quad (39)$$

To compute the adaptive law, we should rewrite (39),

$$\dot{w} = -\lambda e^2 + (y^T - \hat{y}^T)\left(e\psi - \frac{1}{\beta}\dot{\hat{y}}\right) + e\big(\epsilon - \beta sgn(s)\big). \quad (40)$$

If an adaptive law is given by,

$$\dot{\hat{y}} = \beta e\psi, \quad (41)$$

parameters of the fuzzy estimator are obtained as,

$$\hat{y} = \beta \int_0^t e\psi \mathrm{dt} + \hat{y}(0). \quad (42)$$

4. Stability analysis

In this section, quantitative analysis and Bounded Input-Bounded Output (BIBO) analysis are presented for the stability of the closed-loop control system (35).

4.1. Quantitative analysis

According to (41), (40) is re-expressed as,

$$\dot{w} = -\lambda e^2 + e(\varepsilon - \beta sgn(s)), \quad (43)$$

the tracking error reduces if $\dot{w} < 0$. Thus, satisfying $\dot{w} < 0$ results in

$$e(\varepsilon - \beta sgn(s)) < \lambda e^2. \quad (44)$$

According to $e\big(\varepsilon - \beta sgn(s)\big) < |e|(|\varepsilon| + \beta)$, the equation (44) satisfied if,

$$\frac{|\varepsilon|+\beta}{\lambda} < |e|. \quad (45)$$

According to (37), w is a positive definite function, and since $\frac{|\varepsilon|+\beta}{\lambda} < |e|$ then $\dot{w} < 0$. From Lyapunov's theorem, the size of the tracking error reduces until it goes into a ball with a radius $\frac{|\varepsilon|+\beta}{\lambda}$ which means that the tracking error for each joint is ultimately uniformly bounded. The tracking error becomes small if a sufficiently large λ is selected. However, the control law (26) is sensitive to λ such that a significant value makes a massive change in the control effort in the case of a slight change in the tracking error.

4.2. BIBO analysis

The following assumptions are necessary to make the tracking error dynamics well defined such that the robot can follow the desired trajectory.

***Assumption 1*:** The desired trajectory q_d must be smooth in the sense that q_d and its derivatives up to necessary orders are available, and all are uniformly bounded [28].

***Assumption 2*:** The voltage of the electric motor must be bounded, i.e., $|V| < V_{max}$. This assumption safeguards the electric motor against overvoltage.

***Theorem 1*:** By considering Assumption 1 for the closed-loop control system (35), The variables e, $\dot{e}$, q and $\dot{q}$ remain bounded.

***Proof*:** According to (45), e is bounded. On the other hand, the boundedness of q is proved by considering Assumption 1 and (14). In other words, Assumption 1 shows the desired trajectory is bounded and (14) is a linear equation; since e and q_d are bounded, q is bounded. Equation (36) is a linear first-order system; since fuzzy function, estimation error, tracking error, and estimation parameter error are bounded, $\dot{e}$ is bounded. Additionally, from the boundedness of the desired trajectory derivatives $\dot{q}_d$ in Assumption 1, and since $\dot{q} = \dot{q}_d - \dot{e}$ the boundedness of $\dot{e}$ also implies that $\dot{q}$ is bounded.■

***Theorem 2*:** By considering characteristics of Assumption 2, system (8) and controller (26), if $\overline{\Delta H}(I_a, \dot{\theta}_m)$ is bounded then $\mathrm{I_a}$ and $\dot{\theta}_m$ are bounded.

***Proof*:** Assumption 2 indicates that V is bounded, according to (26) and Theorem 1, the boundedness of $V, \dot{e}, e, \beta sgn(s)$ implies that $\overline{\Delta H}(I_a, \dot{\theta}_m)$ is bounded. Therefore, according to (24) since $\overline{\Delta H}(I_a, \dot{\theta}_m)$ is bounded, I_a and $\dot{\theta}_m$ are bounded. ■

***Theorem 3*:** By considering the boundedness of q, I_a and $\dot{\theta}_m$, that proved in Theorem 1 and 2, θ_m is bounded.

***Proof*:** The dynamic equation of actuator is expressed in (5), substituting τ_m (7) into (5) yields,

$$J\ddot{\theta}_m + B\dot{\theta}_m + r^2 K\theta_m = K_m I_a + rKq, \quad (46)$$

since J, B and r^2K are positive diagonal matrices, according to Theorem 1, the linear system expressed by (46) is stable with the bounded input $K_m I_a + rKq$. As a result, the output θ_m is bounded. ■

In summary, all system states are bounded. Thus, it is concluded that the proposed controller guarantees BIBO stability.

5. Result

Simulation and experimental analysis are carried out to verify further the proposed controller's effectiveness on the designed surgical robot. The actuator dynamic plays a fundamental role in this simulation and experimental study. Hence, each joint is separately controlled in the joint space, i.e., the proposed control law (26) is applied to each motor. The vital tip is that the controller is based on a voltage mode control strategy. Table A in Appendix provides the robot's and motors' parameters, and Fig.3 illustrates the block diagram of the proposed approach closed-loop control system. To consider the parametric uncertainty, it is assumed that simulation parameters are about 80% of their actual values provided in Table A in the Appendix.

Each controller's parameters are given in Table B in Appendix, which are determined by the Taguchi optimal method introduces in [29] to achieve reasonable error. The performance index that is used in this paper is Mean Squared Error (MSE) that defined as,

$$MSE = \begin{cases} \frac{1}{T}\int_0^T (e_1^2 + e_2^2 + \cdots + e_9^2)dt \\ \frac{1}{T}\int_0^T (E_1^2 + E_2^2 + E_3^2)dt \end{cases}, \qquad (47)$$

where T is the duration of operation, $e_1, e_2 \ldots e_9$ are the tracking errors for joints 1, 2,… 9, respectively. As well as E_1, E_2 and E_3 are the end effector's tracking error in the Cartesian space.

Also, the control of the surgical robot in the Cartesian space is a significant challenge; therefore, the proposed controller is evaluated in this space for simulation and experimental study.

The computer adopted here is an Intel Core-i7, CPU 2.60 GHz, with 8G RAM to model the robot and produce the surgical simulator. The surgical robot simulation is accomplished by combining the SimMech toolbox of MATLAB with SolidWorks to reach accurate and realistic results.

5.1. Case study 1: Regulator scenario in the joint space

The regulator motion control is a standard test performed in many robotic applications to show the controller's efficiency. The desired joint angles are set to 1 rad to test the proposed controller. Control performances have been satisfactory as the joint angles converge to the desired value with insignificant chattering by minor final error, as shown in Fig.4. The MSE index in this simulation is 0.01947 rad. Fig.5 illustrates that the motors respond quickly with high actuation values within the permitted voltages at the beginning and reduce gently during the simulation; finally, the current of motors is depicted in Fig.6.

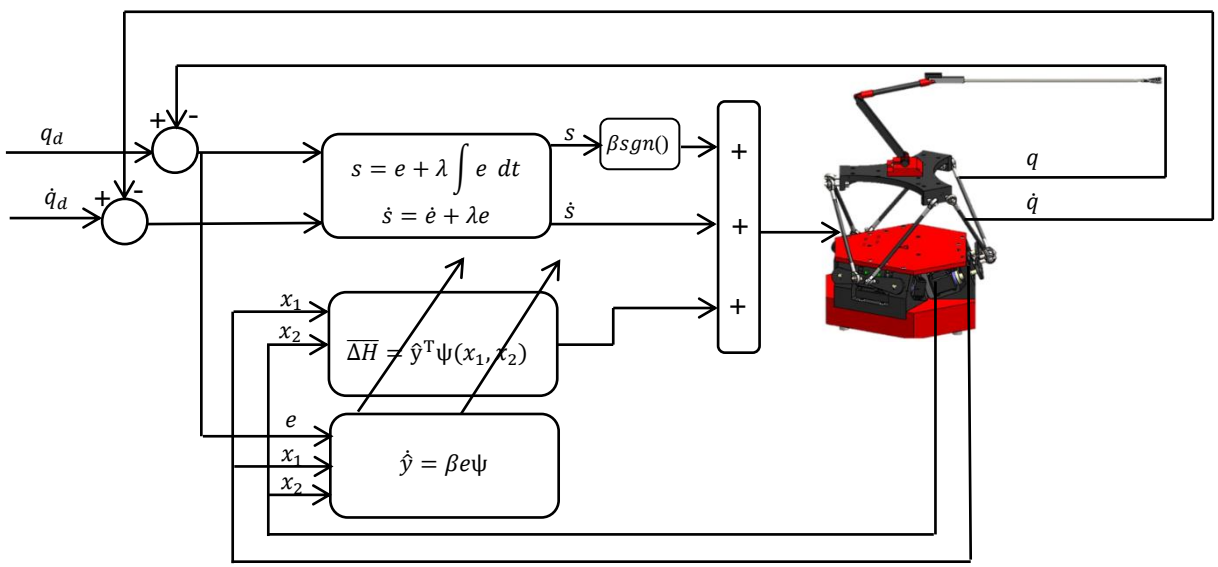

Figure 3. Block diagram of the proposed controller

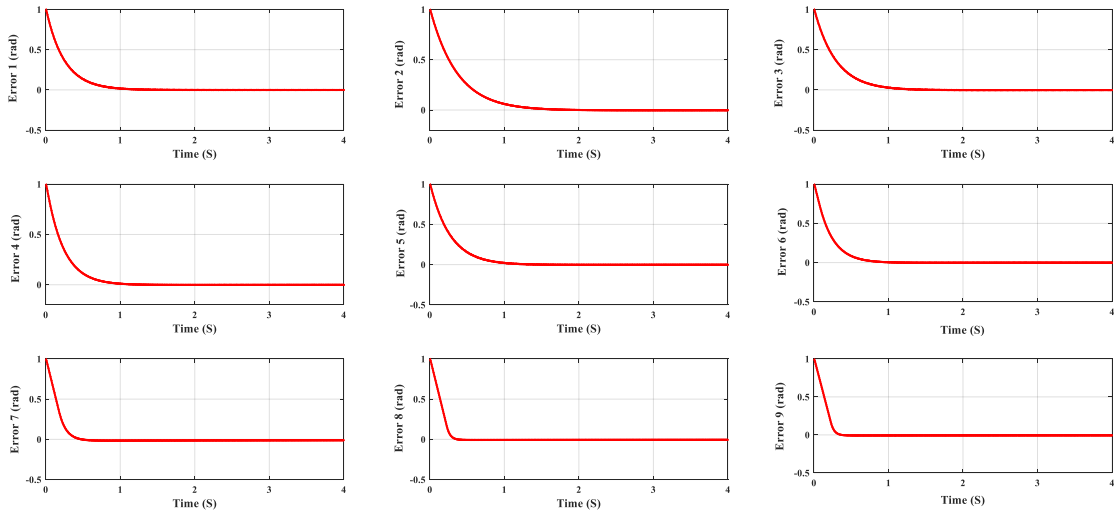

Figure 4. Motor errors for case study 1 (regulator scenario in the joint space)

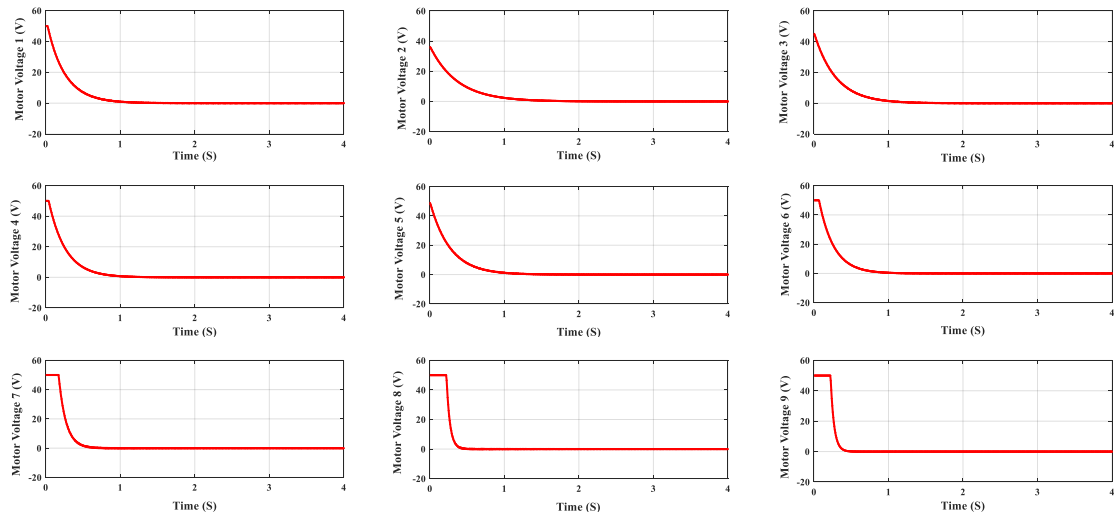

Figure 5. Motor voltages for case study 1 (regulator scenario in the joint space)

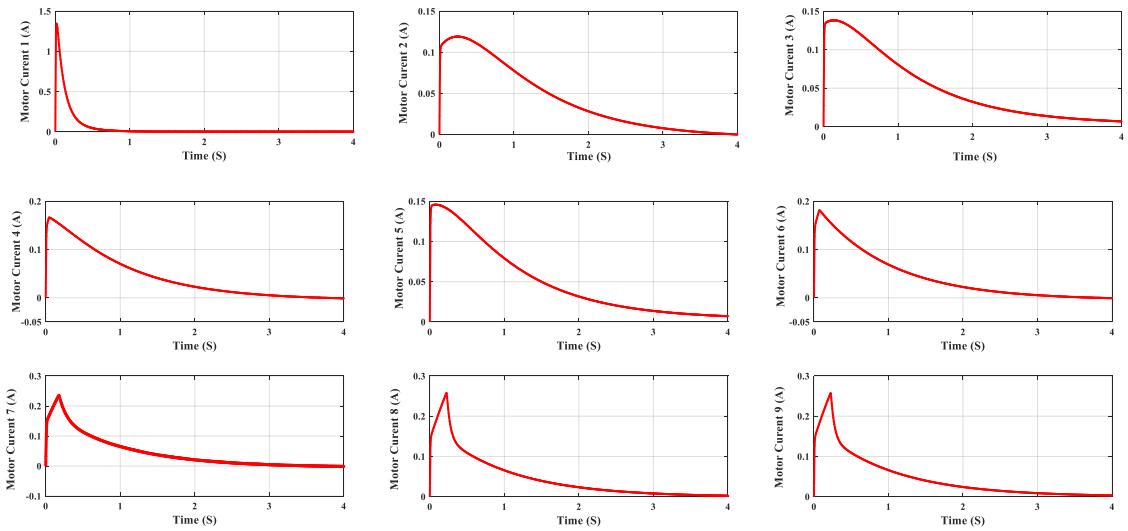

Figure 6. Motor currents for case study 1 (regulator scenario in the joint space)

5.2. Case study 2: Tracking scenario in the joint space

Tracking motion control is another test performed in robotic applications to evaluate the controller's performance. The desired trajectories are sufficiently smooth so that all of its derivatives up to the required order are bounded. The desired trajectory is designed based on the cubic equation for each joint; as a result, it is given by,

$$q_d = \mu T^3 + \vartheta T^2, \qquad (48)$$

where T is the operation's duration, and Table C in Appendix presents the other desired trajectory parameters for each joint and Fig.7 shows these trajectories.

This controller tries to counteract the elasticity and chattering effects in the surgical robot's control, which are fundamental challenges in this area. Fig.8 shows the control system's performance. According to this figure, the performance index should be reduced, and the simulation shows the MSE is 5×10^{-4} rad. As seen in Fig.9, the control efforts behave well within their bounds and without the system chattering phenomenon that appears in the traditional sliding mode controller. Finally, Fig.10 shows the currents of motors.

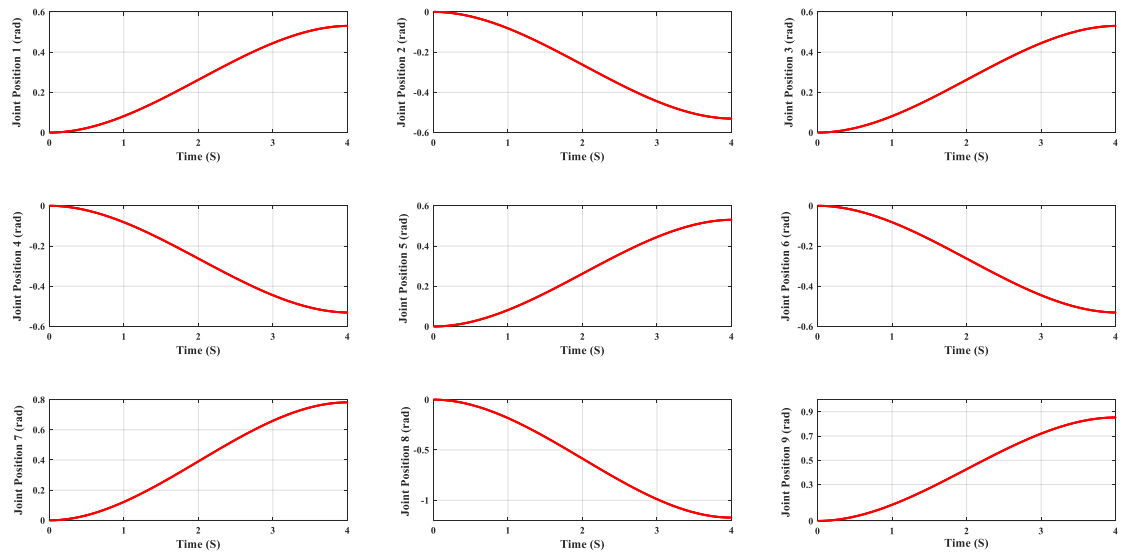

Figure 7. The desired trajectories for case study 2 (tracking scenario in the joint space)

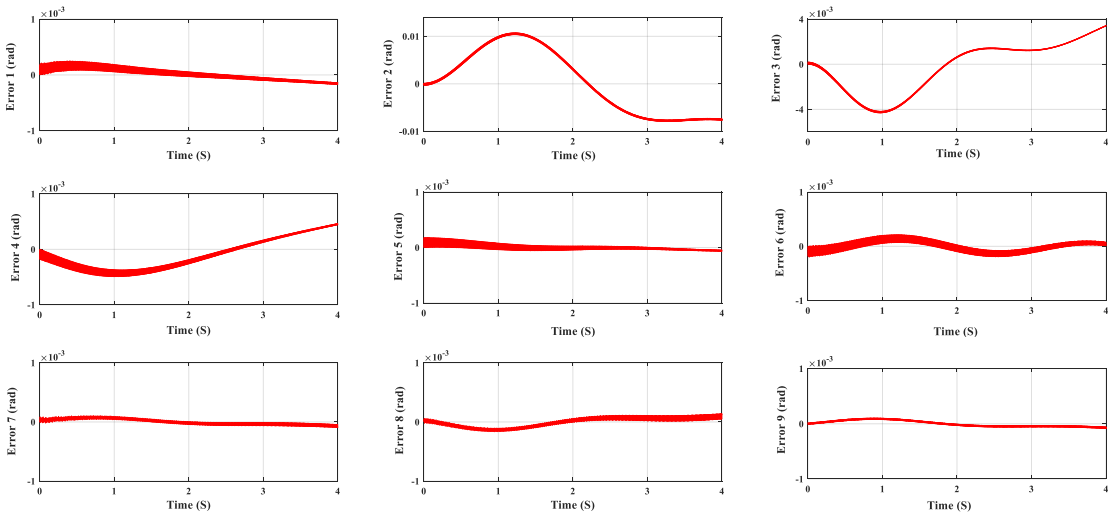

Figure 8. Motor errors for case study 2 (tracking scenario in the joint space)

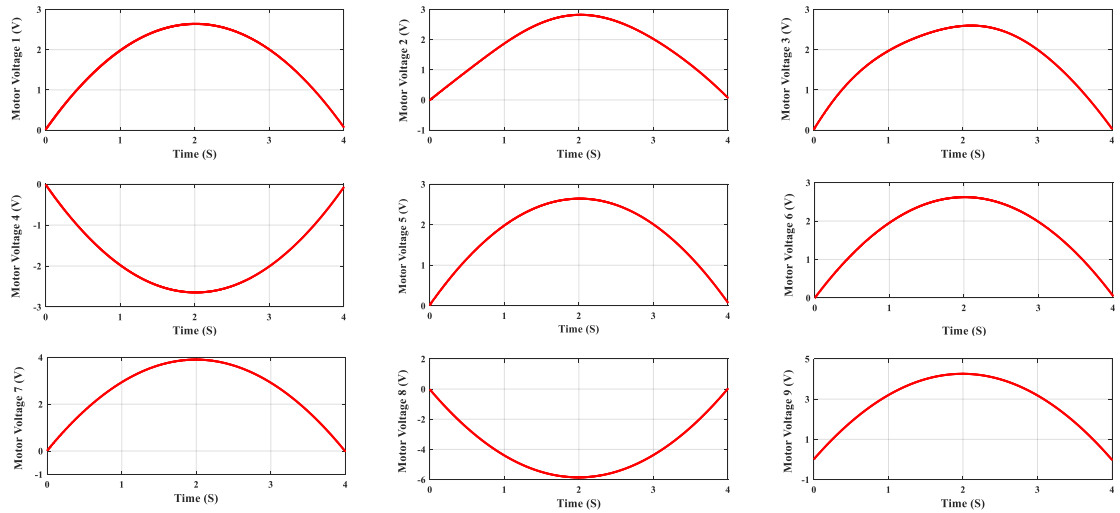

Figure 9. Motor voltages for case study 2 (tracking scenario in the joint space)

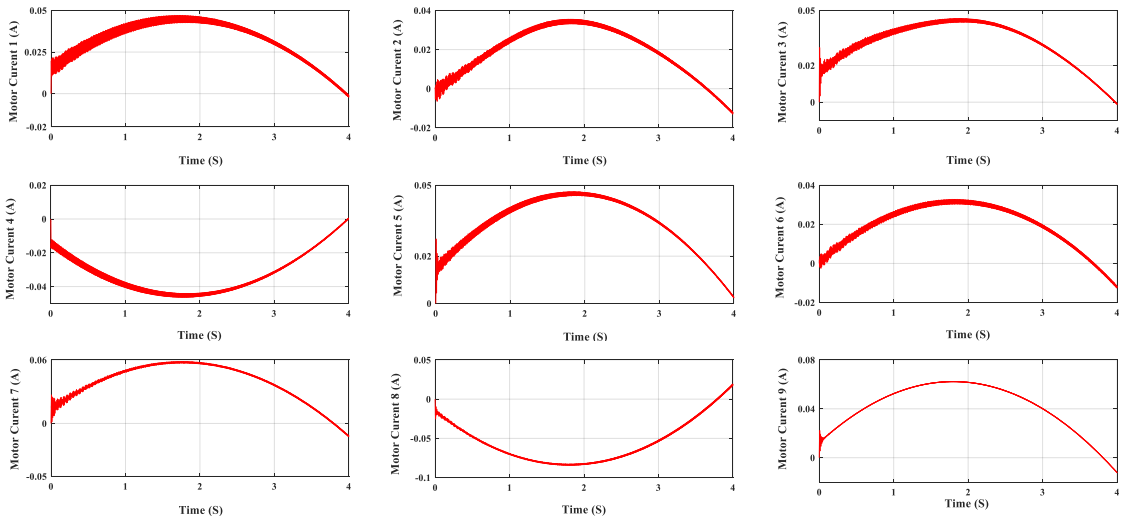

Figure 10. Motor currents for case study 2 (tracking scenario in the joint space)

5.3. Case study 3: Tracking scenario in the Cartesian space

To evaluate the controller's performance, this test is performed for the proposed robot. Similar to the previous simulation, the desired trajectories are sufficiently smooth so that all of its derivatives up to the required order are bounded and defined as,

$$\begin{cases} x_d = -\pi/34T^3 + \pi/5.6T^2 \\ y_d = -\pi/34T^3 + \pi/5.6T^2 + 1, \\ z_d = \pi/34T^3 - \pi/5.6T^2 + 0.5 \end{cases} \quad (49)$$

These trajectories are shown in Fig.11 and Fig.12 shows the control system's performance in x, y, and z axes. The MSE index of the proposed controller is 3×10^{-4} cm in this test. As can be seen, the proposed controller has an acceptable performance in the Cartesian space.

5.4. Case study 4: Comparison

The proposed strategy is compared with the control approach given by [2] because this strategy is simulated on the hybrid surgical robot. This control strategy is based on a remote center-of-motion (RCM) constraint that ignores the dynamics of electric actuators because it is based on torque mode control. As a result, this strategy ignores the joint elasticity. Both control strategies are simulated on this study's elastic joint hybrid surgical robot to have a fair comparison. The tracking trajectories for the end effector of the robot are defined as,

$$\begin{cases} x_d = -\cos(T) \\ y_d = \sin(T) \\ z_d = -\cos(T) \end{cases}, \quad (50)$$

These trajectories are shown in Fig.13. We used the optimal method that introduces in [29] to choose the best parameters for both controllers.

The tracking errors of both controllers are shown in Fig.14, and the simulation shows the MSE index of the proposed controller is 5×10^{-4} cm in this test. Fig.14 (b) shows that the size of tracking errors increase instead of the proposed controller, as well as, the MSE index is increased to 13×10^{-3} cm.

Eventually, the proposed strategy is superior to [2] because the proposed controller is free from robot dynamics and handled this as an external load; on the other hand, it is considered the actuators' dynamic and joint elasticity for a realistic situation.

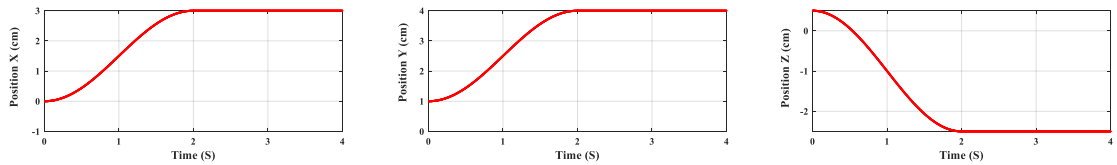

Figure 11. The desired trajectories for case study 3 (tracking scenario in the Cartesian space)

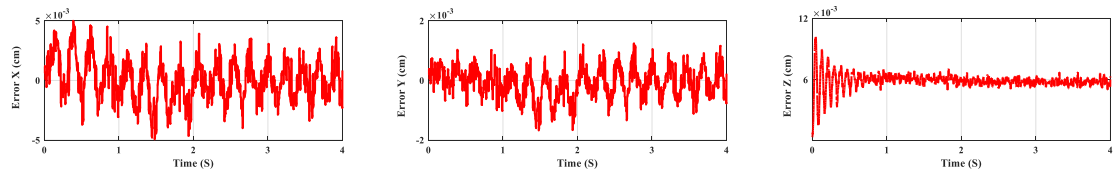

Figure 12. End effector errors for case study 3 (tracking scenario in the Cartesian space)

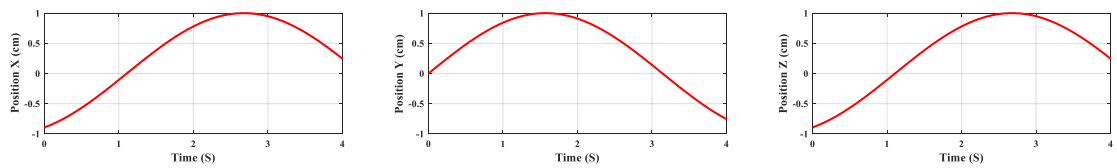

Figure 13. The desired trajectories for case study 4 (comparison scenario in the Cartesian space)

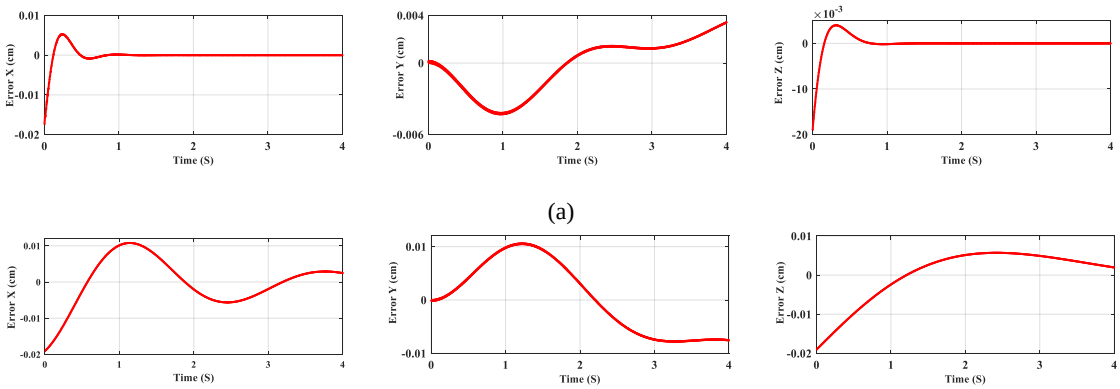

(a)

(b)

Figure 14. End effector errors for case study 4. (comparison in the Cartesian space). (a) the proposed controller, (b) the controller of [2]

5.5. Experimental result

This controller is applied to the hybrid parallel-serial robot at the Ferdowsi University of Mashhad's robotic laboratory to verify the proposed controller performance in feasible implementation. The robot has complexities and uncertainties, such as complicating kinematic and dynamic, joint elasticity, and measurement noise; therefore, the proposed controller can play a vital role in the closed-loop control cycle in both joint and Cartesian space.

The specification of the host computer adopted here is the same as the simulation section. The motors are driven using the "DFrobot L298p Twin V1.1" board, which is an Arduino compatible motor driver. This board is based on an "Atmega328" microcontroller. H-bridges circuit is used for each driving motor, and the PWM signals are produced with an electronic board consisting of an Atmel ATmega328 that runs at 16 MHz clock speed. Nine permanent magnet DC motors are used for this robot. Finally, to provide the position feedback, the internal potentiometer of each motor is used. Also, to stimulate the armature used the two ends of the terminal voltage wire of motors. In other words, 5 wires must be used for each motor: 2 wires for armature voltage and 3 wires for potentiometer. Therefore, the position feedbacks are sent to the host computer to prepare the proposed control law.

According to the existing movements in the surgical operations, the tracking scenario in both joint and Cartesian space is tested in this experiment. The desired trajectories are the same as simulation tests. The schematic diagram of the experimental setup is presented in Fig.15. Fig.16 shows the hybrid parallel-serial robot and explains each part of this robot separately. The controller performance in the joint space is shown in Fig.17, as is evident the MSE index in the experimental test is increased compared to the simulation test, and it is 8×10^{-3} rad. It is necessary to mention that the differences between the experimental and simulation tests are due to the measurements' accuracy. Fig.18 shows the end effector performance in the Cartesian space and the MSE index for this test is 9×10^{-3} cm. According to these figures, the existing chattering does not affect the actuators' and the controllers' performance.

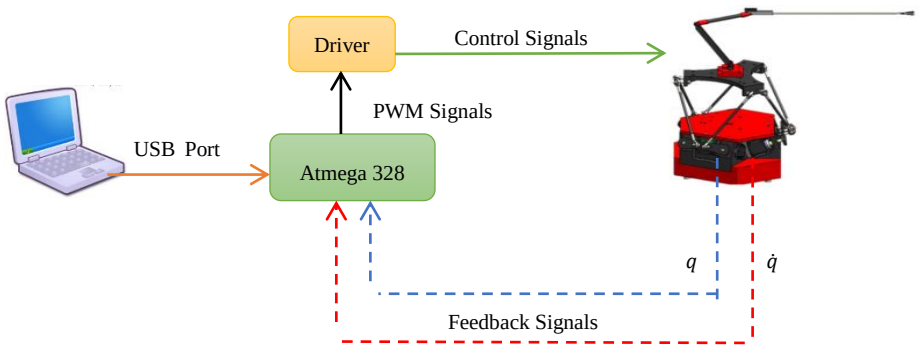

Figure 15. Schematic diagram of the experimental setup

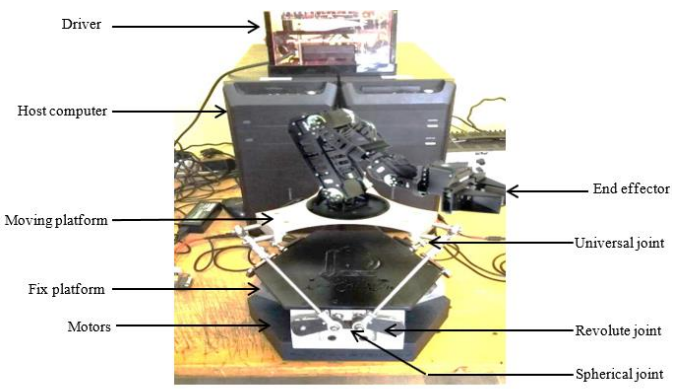

Figure 16. Hybrid surgical robot

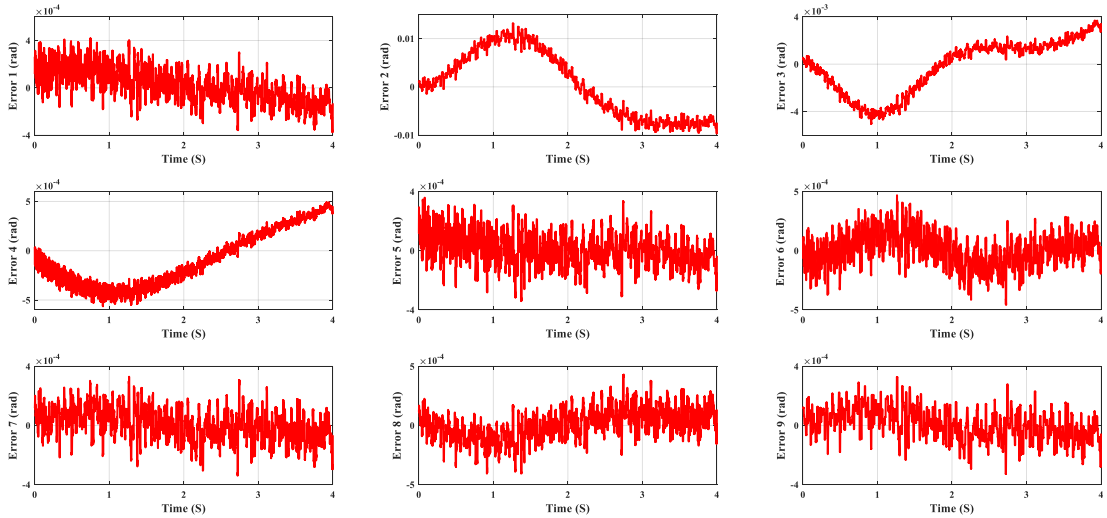

Figure 17. Motor errors for the experimental test in the joint space

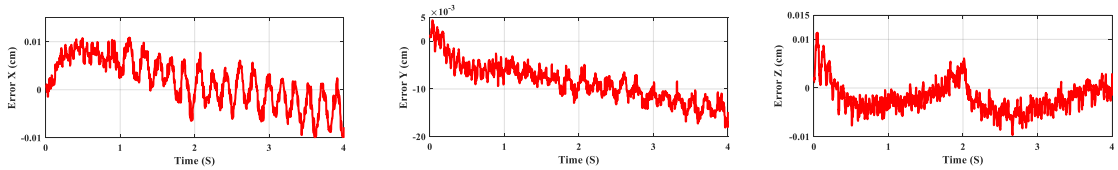

Figure 18. End effector errors for the experimental test in the Cartesian space

6. Conclusions

Parallel robots offer high rigidity and repeatability, while serial manipulators provide a larger workspace and finer manipulability. Surgeons require both of these properties in surgical robotics. Also, confront the added constraint of being small, which leads to joint elasticity as an essential property for medical robots. This paper presents an elastic-joint hybrid parallel-serial surgical robot and introduces a stable sliding mode controller by an indirect adaptive fuzzy estimator based on the voltage mode control strategy. One of this controller's advantages that simplifies the control structure is eliminating the inner current control loop compared to the usual torque-based mode strategies. The closed-loop system's stability is proved by theoretical analysis without requiring the knowledge of the uncertainty bound in robot dynamics. Finally, SolidWork and MATLAB Simulink's interface provides a realistic framework to design and test this complex mechanism. Simulation and experimental results confirm this approach's superiority in following the required trajectory while decreasing the control signals' chattering, which is a common attribute of sliding mode controllers. In the future, we hope to utilize this robot for telesurgery as a master and slave robot that matches their motion in different situations such as contacting and free motion mode by different body tissues in unstructured environments.

Acknowledgments

The authors would like to express their gratitude to the Advanced Robotic Laboratory at the Ferdowsi University of Mashhad and Robotic Laboratory of the Shahrood University of Technology for providing the facilities to implement the experimental tests in this study. Also, we gratitude to Dr. Kalani for his cooperation in the initial design of the proposed robot.

REFERENCES

[1] BiomedHomepage, /http://biomed.brown.eduS, 2015.

[2] M. Moradi Dalvand, B. Shirinzadeh, Motion control analysis of a parallel robot-assisted minimally invasive surgery/microsurgery system (PRAMiSS), Robotics and Computer-Integrated Manufacturing, Vol.29, (2013), 318–327.

[3]H. Maki, Handbook of Research on Biomimetics and Biomedical Robotics- Technology & Engineering, 2017.

[4]S. Divi, S. Pollster, E. Ramos, J. Lee, The Current Role of Robotic Technology in Spine Surgery, Operative Techniques in Orthopaedics, Vol.27, (2017) 275-282.

[5] D. Zhijiang , L. Yunlei, Y. Zhiyuan, S. Lining, C. Wei, Human-robot interaction control of a haptic master manipulator used in laparoscopic minimally invasive surgical robot system, Mechanism and Machine Theory, Vol.156, (2021), 104-132.

[6] S. Jonas, R. Dominiek, V. Emmanuel, Synthesis and methodology for optimal design of a parallel remote center of motion mechanism: Application to robotic eye surgery, Mechanism and Machine Theory, Vol.151, (2020).

[7] F. Lukasz, S. Mateusz, P. Leszek , Share control of surgery robot master manipulator guiding tool along the standard path, The International Journal of Medical Robotics and Computer Assisted Surgery, Vol.15(3), (2019).

[8]H. Li, W. Liu, K. Wang, K. Kawashima, E. Magid, A cable-pulley transmission mechanism for surgical robot with back drivable capability, Robotic and Computer-Integrated Manufacturing, Vol.49, (2018), 328 334.

[9] J. Danielle, Developing an Intelligent Tutoring System for Robotic-assisted Surgery Instruction, The International Journal of Medical Robotics and Computer Assisted Surgery, (2019).

[10]M.M. Fateh, M. Souzanchi-K, Indirect adaptive fuzzy control for flexible-joint robot manipulators using voltage control strategy, Journal of Intelligent & Fuzzy Systems, Vol.28, (2015) 1451-1459.

[11]M.M. Fateh, M. Souzanchi-K, Decentralized direct adaptive fuzzy control for flexible joint robots, Journal of Control Engineering and Applied Informatics, Vol.15, (2013) 97-105.

[12]S.M. Ahmadi, M.M. Fateh, Task-space asymptotic tracking control of robots using a direct adaptive Taylor series controller, Journal of Vibration and Control, Vol.24(23), (2018), 5570-5584.

[13] M. Souzanchi-K, A. Arab, M-R. Akbarzadeh-T, M.M. Fateh, Robust Impedance Control of Uncertain Mobile Manipulators Using Time Delay Compensator, IEEE Transactions on Control Systems Technology, Vol.26(6), (2018), 1942-1953.

[14]V. Khoshdel, A. Akbarzadeh, N. Naghavi, A. Sharifnezhad, M. Souzanchi-K, sEMG-based impedance control for lower-limb rehabilitation robot, Intelligent Service Robotics, Vol.11, (2018) 97-108.

[15]R. Gholipour, M.M. Fateh, Adaptive task-space control of robot manipulators using the Fourier series expansion without task-space velocity measurements, Measurement, Vol.123, (2018), 285-292.

[16]A. Izadbakhsh, S. Khorashadizadeh, Robust adaptive control of robot manipulators using Bernstein polynomials as universal approximator, International Journal of Robust and Nonlinear Control, Vol.30 (7), (2020), 2719-2735.

[17]M. Vijay, D. Jena, Backstepping terminal sliding mode control of robot manipulator using radial basis functional neural networks, Computers & Electrical Engineering, Vol.67, (2018), 690-707.

[18]G. Chen, B. Jin, Y. Chen, Nonsingular fast terminal sliding mode posture control for six-legged walking robots with redundant actuation, Mechatronics, Vol.50, (2018), 1-15.

[19]S. Chegini, M. Yarahmadi, Quantum sliding mode control via error sliding surface, Journal of Vibration and Control, Vol.24(22), (2018), 5345-5352.

[20] M. Souzanchi-K, M-R Akbarzadeh-T, Brain Emotional Learning Impedance Control of Uncertain Nonlinear Systems with Time Delay: Experiments on a Hybrid Elastic Joint Robot in Telesurgery, Computer in biology and medicine, Accepted, (2021).

[21]Y. Bouteraa, I.B. Abdallah, J. Ghommam, Task-space region-reaching control for medical robot manipulator, Computers & Electrical Engineering, Vol.67, (2018), 629-645.

[22] I. Zaplana, L. Basanez, A novel closed-form solution for the inverse kinematics of redundant manipulators through workspace analysis, Mechanism and Machine Theory, Vol.121, (2018), 829-843.

[23] A.M. Ghalamzan, M. Ragaglia, Robot learning from demonstrations: Emulation learning in environments with moving obstacles, Robotics and Autonomous Systems, Vol.101, (2018), 45-56.

[24] Y. Abdullah, K. Gökhan, Kinematic design of a non-parasitic 2R1T parallel mechanism with remote center of motion to be used in minimally invasive surgery applications, Mechanism and Machine Theory, Vol.153, (2020), 104-132.

[25] H. Zhang, S. Chen, W. Wang, J. Zhang, G Zong, Runtime reconfiguration of a modular mobile robot with serial and parallel mechanisms, IEEE/RSJ Int. Conf. Intell. Robot. Syst., San Diego, USA, (2007), 2999– 3004.

[26] M. Spong, S. Hutchinson, M. Vidyasagar, Robot Modelling and Control, John Wiley & Sons, NY, USA, 2006.

[27] L.X A. Wang, Course in Fuzzy Systems and Control, Prentice-Hall International, NJ, USA, 1997.

[28] Z. Qu, D.M. Dawson, Robust Tracking Control of Robot Manipulators, IEEE Press, NY, USA, 1996.

[29] V. Khoshdel, A. Akbarzadeh, Application of statistical techniques and artificial neural network to estimate force from sEMG signals, Journal of AI and data mining, Vol.4, (2016), 135-141

Appendix

Table A. Parameters of robot and motors

	parameter	Mass (gr)	Center of mass (mm)	Moment of inertia $(kg \times m^2)$
Parallel robot	Base platform	1000	[0 0 0] (point mass)	[1 1 1]
	Leg1-6	70	[-40.12 81.73 -7.48]	[167306.28 48185.87 4677.28]*10e-9
	Moving platform	707.15	[0 0.02 -8.92]	[2307825.70 2308639.32 4553681.14]*10e-9
Serial robot	Base1	150	[0.57 0 8.20]	[46120.81 35483.43 71961.86]*10e-9
	Link7	80	[72.5 0 0]	[967.81 41228.56 41193.82]*10e-9
	Link8	45	[65.35 0.1 0]	[253.59 23045.94 23033.14]*10e-9
	Link9	30	[13.74 5 0]	[283.80 4096.10 4281.3]*10e-9

Motor	K	r	R	L	k_b	B_m	J_m	$V_{\max}$
	$(\frac{Nm}{rad})$		(Ω)	(mH)	$(\frac{Vs}{rad})$	$(\frac{Nms}{rad})$	$(\frac{Nms^2}{rad})$	(V)
	500	0.02	1.6	1	0.26	0.001	0.0002	50

Table B. Parameters of controllers

Workspace	Scenario	Controller	1&2	3&4	5&6	7&8&9
Joint Space	Regulator	λ	85	94	100	70
		β	0.03	0.09	0.07	0.05
	Tracking	λ	130	112	100	140
		β	0.04	0.02	0.08	0.05
Cartesian Space	Tracking	λ	104	97	83	134
		β	0.03	0.015	0.064	0.48

Table C. Parameters of desired trajectories in joint space

Joint	1&3&5	2&4&6	7	8	9
μ	$-\pi$ /193	π /193	$-\pi$ /128	π /85	$-\pi$ /118
ϑ	π /32	$-\pi$ /32	π /21	$-\pi$ /14	π /20

Biography

Mahdi Souzanchi-K. received the B.Sc. and M.Sc. degrees in Robotic and Control Engineering from the University of Shahrood, Shahrood, Iran, in 2011 and 2013, respectively. He is currently pursuing a Ph.D. degree in control engineering. Since 2014, he has been a research fellow with the Center of Excellence on Soft Computing and Intelligent Information Processing (SCIIP), Ferdowsi University of Mashhad, Mashhad, Iran. His research interests include robotics and intelligent systems, control robot, fuzzy control, and human-robot interaction.

Mohammad-R. Akbarzadeh-T. received his Ph.D. degree from the University of New Mexico (UNM), Albuquerque, NM, USA, in 1998. He is currently a professor and director of Center of Excellence on Soft Computing and Intelligent Information Processing, departments of electrical engineering and computer engineering, Ferdowsi University of Mashhad, Mashhad, Iran. Prof. Akbarzadeh is the founding president of the Intelligent System Scientific Society of Iran. He is a senior member of the IEEE, a life member of Eta Kappa Nu (The Electrical Engineering Honor Society), and Kappa Mu Epsilon (the mathematics Honor Society). His research interests are in the areas of bio inspired computing/optimization, fuzzy logic and control, soft computing, multi-agent system, complex system, robotic, cognitive science and medical informatics. He has published over 450 peer-reviewed articles in this and relates research fields.